

# The superconducting twin qubit

I. V. Antonov,<sup>1,2</sup> R. S. Shaikhaidarov,<sup>1</sup> V. N. Antonov,<sup>3,1,4</sup> and O.V. Astafiev<sup>3,1,2</sup>

<sup>1</sup>Royal Holloway, University of London, Egham, TW20 0EX, UK

<sup>2</sup>National Physical Laboratory, Hampton Road Teddington, TW11 0LW, UK

<sup>3</sup>Skolkovo Institute of Science and Technology, Nobel str. 3, Moscow, 143026, Russia

<sup>4</sup>Moscow Institute of Physics and Technology, 29 Institutskiy per., 141700 Dolgoprudny, Moscow Region, Russia

(Dated: January 27, 2020)

In this work we study a modification of a flux ‘‘twin-qubit’’ geometry – a combination of two loops joined by a common Josephson junction, which can potentially have some advantages with other devices. At the degeneracy flux-bias point,  $\Phi_0/2$ , the twin qubit has energy spectrum plateaus and anharmonicity, more than 2 GHz. This flatness makes the qubit insensitive to a global low-frequency flux noise. The qubit is capacitively coupled to a transmission line, which allows to experimentally measure its spectrum. Our simulations reproduce the measured spectrum.

Keywords: Flux-qubit

Superconducting qubits are one of the most promising platforms for quantum computing technology. Typical qubits are on-chip aluminum structures with Josephson junctions (JJs), whose geometry can be designed to select an operating energy, state transition rates and sensitivity required in a particular environment. Over the past decade they have carried out the functionality of a transistor [1–4], where a control field was used to pass or block a probe field at a different frequency, multiplexer [5], two input signals can be mixed to controllably generate a single output signal, and serial bus [6]. Superconducting qubits can be fabricated using standard nanofabrication techniques and integrated at scale into quantum circuits [7].

One of the inherent limitations, which is encountered with superconducting qubits, is a coherence time,  $\tau_{\text{dec}}$ , beyond which quantum information becomes lost. Two main sources of de-coherence are charge and flux fluctuations in vicinity of the qubit. Charge fluctuations are particular harmful for the qubits, where the charging energy,  $E_C$ , is large. In flux qubit architectures the JJ energy  $E_J$  dominates over the charging energy  $E_C$  ( $E_J/E_C \gg 1$ ), which lowers the device’s charge sensitivity [8–10]. Therefore a family of flux qubit designs have led to improvement of the coherence times: shunted flux qubit [11], 4-JJ qubit [12, 13].

Here we investigate experimentally a ‘twin’ qubit, consisting of two symmetrical flux qubits, linked by a common  $\alpha$ -Josephson Junction (Fig. 1). Of particular interest to us is the weak flux dependence of the system transition energy when it is biased to the degeneracy point  $\Phi_0/2$  in each loop, making it benefit from low flux fluctuation sensitivities. A chain of 15 such qubits was recently placed into a coplanar waveguide to demonstrate flux-tunable transmission of microwaves [14].

We isolate single twin qubits in the chain, replace inductive coupling by a capacitive one and couple the qubits to the transmission line. Experimental study of the transmission spectrum reveals: weak flux dependence of the transition energies close to the degeneracy point; matching of the experimental energy spectrum with sim-

ulations; anharmonicity with respect to the  $|1\rangle \leftrightarrow |2\rangle$  and  $|2\rangle \leftrightarrow |3\rangle$  transitions.

The sample is fabricated on an undoped silicon substrate, which is pre-patterned with 100 nm Au ground planes. We use electron beam lithography and a shadow evaporation technique to fabricate the qubit shown in Fig. 1(a). It consists of five JJs integrated into two symmetrical superconducting loops. The JJ have a layered structure of Al (20 nm) -  $\text{AlO}_x$  - Al (30 nm). The energy and capacitance of the central JJ is a factor of  $\alpha$  larger than for the outside ones, which have dimensions  $400 \times 200 \text{ nm}^2$ . The coplanar transmission line with impedance  $Z_0 \sim 50 \Omega$  runs to the opening between the ground planes in the center of the chip. The qubits are coupled to the transmission line through T-shaped capacitors. An external magnetic field is applied to change magnetic flux bias in the identical loops.

The sample is mounted on a holder at the 13 mK stage of a dilution refrigerator. A superconducting shield is used to screen the holder from stray magnetic fields. The RF lines connected to the sample have attenuators for thermalization: -50 dBm on the 50 K stage, -30 dBm on the 4 K stage. We attach a circulator on the output line for isolation. The transmitted signal is amplified by approximately +35 dBm on the 4 K stage and by +35 dBm at room temperature. This set of attenuators and amplifiers facilitate power conversion between the laboratory equipment and the qubit. Prior to characterizing the qubit, we took the microwave transmission spectrum with the qubit detuned, and correct all measurements by subtracting background transmission profile.

Our primary goal is to study the operation of the qubit in a double degeneracy point  $\Phi_0/2$ , find the intrinsic energy structure and compare with a numerical model of the system.

We study the energy spectrum of the twin qubit by measuring transmission of coherent waves, while sweeping the biasing magnetic flux. The  $|1\rangle \leftrightarrow |2\rangle$  transition, is mapped with a network analyser which measures the transmission of signal  $\omega_{\text{NA}}$  through the system. Away from resonance the signal passes through the circuit with-

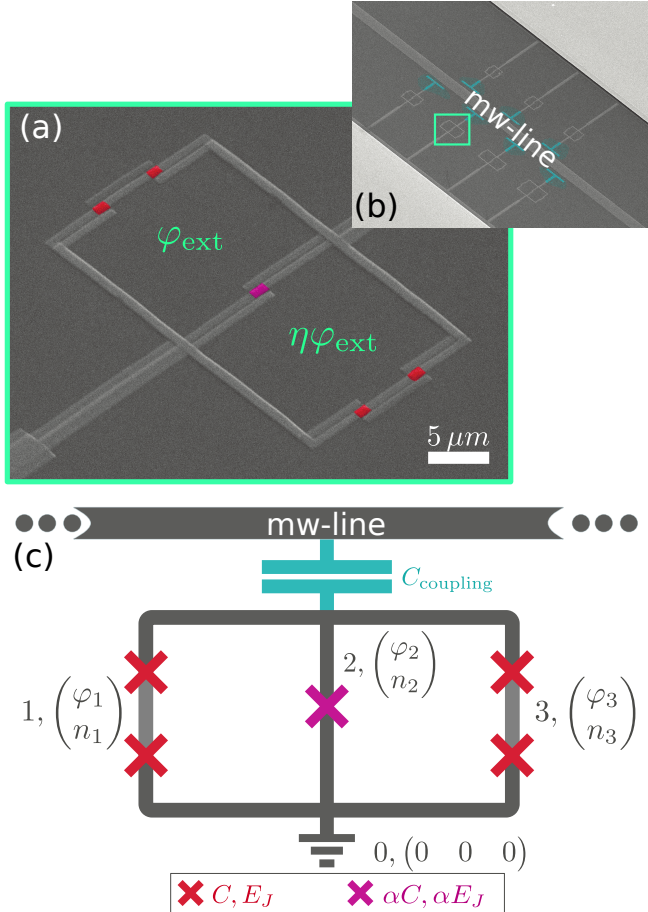


**FIG. 1. Geometry of a twin qubit:** (a) Scanning electron microscope image of the twin qubit. The Al-AlO<sub>x</sub>-Al JJs are highlighted in red and pink; (b) Each of the qubits is coupled to the transmission line with a T-shaped capacitor; (c) The twin qubit is a symmetrical arrangement of two individual flux qubits (as described in Ref. [[8]]) sharing the central JJ. Islands are labeled with a Cooper pair occupation  $n_i$ , phase  $\varphi_i$ , with the ground setting a reference of 0 for the variables. JJs (marked with crosses) mediate capacitive and Josephson interactions between the islands.

out any interaction with the qubit so that the transmission is close to 100%. Only near resonance ( $\omega_{NA} = \omega_{21}$ ), does the qubit exchange photons with the driving field as it evolves between the ground and excited states. The qubit emits a wave that is in anti-phase with the driving field [3], so that the destructive interference in the output line results in a transmission dip, see Fig. 2 inset. The plot shows power transmission  $|t|^2$  obtained in a low limit drive and fitted by a Lorentzian curve with  $\Delta\omega/2\pi \approx 25$  MHz FWHM. This gives us the dephasing rate  $\Gamma_2 \approx \Delta\omega/2 = 79$  MHz [1].

The transmission minimum at different magnetic fields maps out the qubit's  $\omega_{21}$  transition spectrum, Fig. 2(a). Such a spectrum is observed in vicinity of external flux bias  $\Phi \approx \Phi_0/2$  for all samples. Because of a small asymmetry,  $\eta \approx 1$ , the fluxes linked through the left and right

loops can be slightly different:  $\Phi$  and  $\eta\Phi$ , correspondingly. Eventually this results in gradual change of transmission frequency at large magnetic field, Fig 2(b).

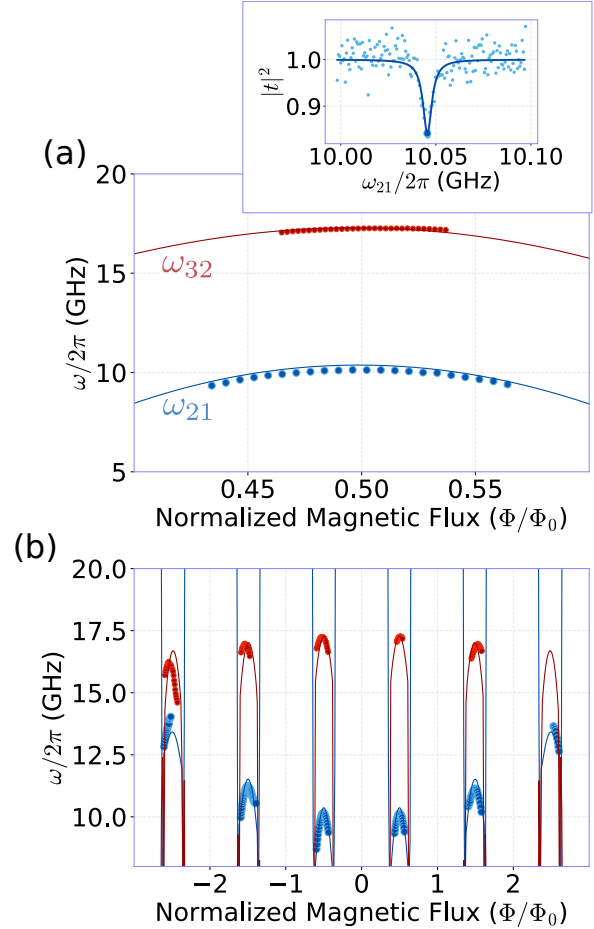


**FIG. 2. Spectrum of the quantum system.** (a) The resonance frequencies,  $\omega_{21}$ , in the vicinity of  $\Phi_0/2$  (blue points). An inset exemplifies the power transmission coefficient  $|t|^2$  for the  $|1\rangle \leftrightarrow |2\rangle$  transition. The transition frequencies  $\omega_{32}$  (red) are obtained in a two-tone measurement. (b) The spectrum measured in a wide flux bias range. Experimental data (circles) are compared with simulations (solid lines) for  $\omega_{21}$  (blue) and  $\omega_{32}$  (red). Asymmetry in the flux penetrating the left and right loops results in the gradual change of transition frequencies with every  $\Phi_0$  period:  $\omega_{21}$  creeps up, while  $\omega_{32}$  creeps down, breaking the usual periodicity of flux qubits.

The  $|2\rangle \leftrightarrow |3\rangle$  transition,  $\omega_{32}$ , is mapped using spectroscopy with two tones. The network analyzer probes signals at  $\omega_{21}$ , while an additional generator sweeps a second frequency,  $\omega_{GEN}$ . Whenever the second tone from the generator hits the  $|2\rangle \rightarrow |3\rangle$  transition ( $\omega_{GEN} = \omega_{32}$ ), the qubit undergoes a ladder of excitations,  $|1\rangle \xrightarrow{\omega_{21}} |2\rangle \xrightarrow{\omega_{32}} |3\rangle$ , depopulating states  $|1\rangle$  and  $|2\rangle$ . Because of this depopulation, the probe signal at  $\omega_{21}$  is modified. This identifies  $\omega_{32}$ , which is mapped with red circles, see Fig 2(b). One can note that the qubit has a large anharmonicity in the two lowest transitions of more than

7.5 GHz.

We match the experimental data to the theoretical model: Islands, isolated by the JJ in Fig. 1, are labeled with Cooper pair (CP) occupation  $\vec{n} = |n_1, n_2, n_3\rangle$ , phase  $\vec{\varphi} = |\varphi_1, \varphi_2, \varphi_3\rangle$  states. The charges and potentials on the islands are linked by the capacitance matrix:

$$2e\vec{n} = \hat{C}\vec{V}. \quad (1)$$

The capacitance matrix in the twin qubit topology is:

$$\hat{C} = |C| \begin{pmatrix} 2 & -1 & 0 \\ -1 & 2 + \alpha & -1 \\ 0 & -1 & 2 \end{pmatrix}, \quad (2)$$

where  $|C|$  is the capacitance of the outer JJs. The interaction of the CPs, carrying a charge  $\vec{Q} = 2e\vec{n}$ , and potentials on their respective islands gives rise to the 'potential' term of the Hamiltonian:

$$U = \frac{1}{2} \sum_{i=1}^3 Q_i V_i = \frac{(2e)^2}{2} \vec{n} \hat{C}^{-1} \vec{n}^T = E_C \sigma_{n_1, n_2, n_3}, \quad (3)$$

where we define  $E_C = (2e)^2/2|C|$  and  $\sigma_{n_1, n_2, n_3} = |C| \vec{n} \hat{C}^{-1} \vec{n}^T$ .

Each JJ with a phase difference of  $\Delta\varphi_i$ , contributes an energy of  $E_{Ji}(1 - \cos(\Delta\varphi_i))$ . The flux quantization condition for the left and right loops,  $\sum_i^{\text{loop}} \varphi_i = 2\pi n, n \in \mathbb{Z}$ , enters as a dependence on  $\varphi_{\text{ext}}$  and  $\eta\varphi_{\text{ext}}$  on two of the junctions:

$$T = E_J [4 + \alpha - \alpha \cos(\varphi_2) - \cos(\varphi_1) - \cos(\varphi_3) - \cos(\varphi_2 - \varphi_1 - \varphi_{\text{ext}}) - \cos(\varphi_2 - \varphi_3 + \eta\varphi_{\text{ext}})]. \quad (4)$$

The Hamiltonian,  $\mathcal{H} = U + T$ , is written in the charge basis (see Supplementary Notes) with  $E_J/h = 91.0$  GHz,  $E_C/h = 13.5$  GHz,  $\alpha = 1.023$ ,  $\eta = 1.011$ . The resulting eigenenergies are compared with the experimental data in Fig. 2. Data for  $\omega_{32}$  is taken in a narrow flux range because away from  $\Phi = (n + \frac{1}{2})\Phi_0, n \in \mathbb{Z}$ , it gets harder to tune the VNA to  $\omega_{21}$  in two-tone spectroscopy. The asymmetry value,  $\eta$ , is close to the 3% seen from the SEM image in Fig. 1. The resonance is periodic in flux, with a tendency of higher  $\omega_{21}$  at higher magnetic flux numbers, because of the loop asymmetry.

An important parameter of the twin qubit is the curvature at the operation point of the qubit,  $\Phi_0/2$ . A low curvature is desirable, because it makes the qubit less sensitive to external flux changes and improves decoherence time. At the twin qubits' degeneracy points  $\Phi = (n + \frac{1}{2})\Phi_0, n \in \mathbb{Z}$ , the curvature is  $(-550 \pm 10)$  GHz/ $\Phi_0^2$ . It is substantially smaller than for 3-JJ and 4-JJ flux qubits with similar JJ parameters, where the curvature is of the order of  $10^5$  GHz/ $\Phi_0^2$  [1, 15, 16].

Figure 3 shows simulation results for an ideal case of fully symmetric system ( $\eta = 1$ ). The curves are exactly periodic in magnetic field with period of  $\Phi_0$ , therefore only one period is shown. The transition energies in

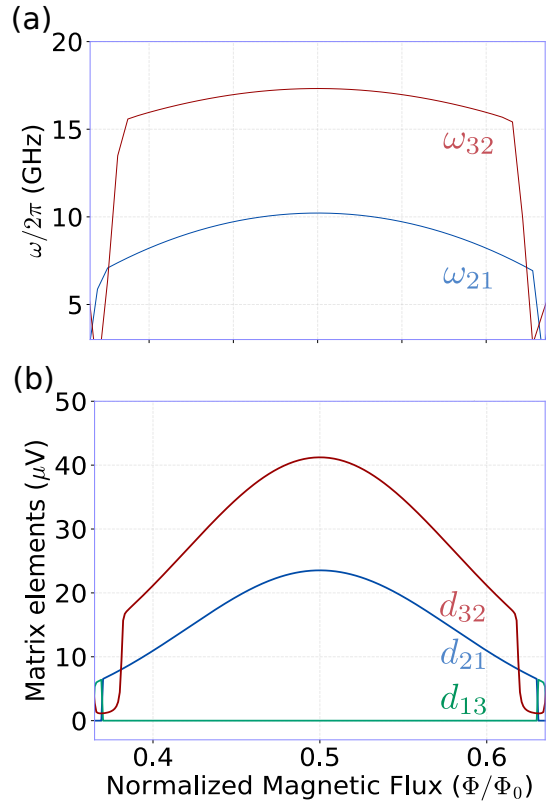


FIG. 3. **Modelling the qubit.** (a) Calculations are done for symmetric qubit. (b) Transition matrix elements  $|d_{12}|$ ,  $|d_{13}|$  and  $|d_{21}|$  for the central island (Fig 1).

Fig. 3(a) are close to the experimental ones. The operational range of the qubit ranges approximately from 0.4 to 0.6 of  $\Phi_0$ , where  $\alpha$ -junction is in the superposed 0- $\pi$  state[14]. Away from that range the transition frequency  $\omega_{21}$  is too high.

Transition matrix elements  $d_{12} = \langle 1 | \hat{V}_2 | 2 \rangle$ ,  $d_{13} = \langle 1 | \hat{V}_2 | 3 \rangle$  and  $d_{21} = \langle 2 | \hat{V}_2 | 3 \rangle$ , which have meaning of induced potential on the island 2 due to excitations, are calculated and plotted in Fig. 3(b). Here the potential operator on the island 2 is  $\hat{V}_2 = \frac{\partial H}{\partial q_2}$ , which is shown in the **Supplement Notes** to be:

$$\delta V_2 = \langle 1 | \frac{E_C}{2|e|(1+\alpha)} [\hat{n}_1 + 2\hat{n}_2 + \hat{n}_3] | 2 \rangle. \quad (5)$$

Finally, we measure Rabi oscillations, see Fig. 4. The oscillations decay with characteristic time  $\tau_{\text{dec}} = 42$  ns, It is the decoherence time taken from the spectroscopy measurements  $\Gamma_2 \approx 1/\tau_{\text{dec}}$  (Fig. 4). A small decoherence time can be a result of poisoning of the sample with the infrared radiation, and the coupling of the two-level oscillators in the substrate, owing to the simplified technology used in the qubit's fabrication. Note also that the decay can not be long and is additionally limited due to strongly coupling to the open line.

In conclusion, we have fabricated and characterized an isolated twin qubit. It has weak flux sensitivity at degen-

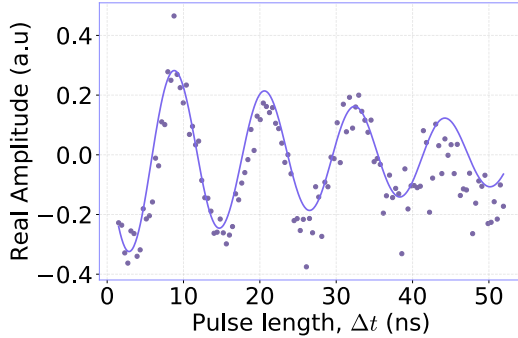


**FIG. 4. Rabi oscillations:** taken at the degeneracy point by driving the qubit with resonant microwaves pulses for fixed time periods,  $\Delta t$ . The decoherence time of  $\tau_{\text{dec}} = 42 \text{ ns}$  is extracted from the decay envelope,  $e^{-\Delta t/\tau_{\text{dec}}}$ , of the the oscillations.

eracy points and strong anharmonicity. The measured energy level structure is well reproduced by the numerical model.

- 
- [1] O. Astafiev, A. M. Zagoskin, A. A. Abdumalikov, Y. A. Pashkin, T. Yamamoto, K. Inomata, Y. Nakamura, and J. S. Tsai, Resonance fluorescence of a single artificial atom, *Science* **327**, 840 (2010).
- [2] I.-C. Hoi, C. M. Wilson, G. Johansson, T. Palomaki, B. Peropadre, and P. Delsing, Demonstration of a single-photon router in the microwave regime, *Physical Review Letters* **107**, 10.1103/physrevlett.107.073601 (2011).
- [3] A. A. Abdumalikov, O. Astafiev, A. M. Zagoskin, Y. A. Pashkin, Y. Nakamura, and J. S. Tsai, Electromagnetically induced transparency on a single artificial atom, *Physical Review Letters* **104**, 10.1103/physrevlett.104.193601 (2010).
- [4] O. V. Astafiev, A. A. Abdumalikov, A. M. Zagoskin, Y. A. Pashkin, Y. Nakamura, and J. S. Tsai, Ultimate on-chip quantum amplifier, *Physical Review Letters* **104**, 10.1103/physrevlett.104.183603 (2010).
- [5] T. Höngl-Decrinis, I. V. Antonov, R. Shaikhaidarov, V. N. Antonov, A. Y. Dmitriev, and O. V. Astafiev, Mixing of coherent waves in a single three-level artificial atom, *Physical Review A* **98**, 10.1103/physrev.a.98.041801 (2018).
- [6] J.-T. Shen and S. Fan, Coherent single photon transport in a one-dimensional waveguide coupled with superconducting quantum bits, *Physical Review Letters* **95**, 10.1103/physrevlett.95.213001 (2005).
- [7] M. W. Johnson, P. Bunyk, F. Maibaum, E. Tolkaheva, A. J. Berkley, E. M. Chapple, R. Harris, J. Johansson, T. Lanting, I. Perminov, E. Ladizinsky, T. Oh, and G. Rose, A scalable control system for a superconducting adiabatic quantum optimization processor, *Superconductor Science and Technology* **23**, 065004 (2010).
- [8] T. P. Orlando, J. E. Mooij, L. Tian, C. H. van der Wal, L. S. Levitov, S. Lloyd, and J. J. Mazo, Superconducting persistent-current qubit, *Physical Review B* **60**, 15398 (1999).
- [9] I. Chiorescu, Coherent quantum dynamics of a superconducting flux qubit, *Science* **299**, 1869 (2003).
- [10] J. E. Mooij, Josephson persistent-current qubit, *Science* **285**, 1036 (1999).
- [11] F. Yan, S. Gustavsson, A. Kamal, J. Birenbaum, A. P. Sears, D. Hover, T. J. Gudmundsen, D. Rosenberg, G. Samach, S. Weber, J. L. Yoder, T. P. Orlando, J. Clarke, A. J. Kerman, and W. D. Oliver, The flux qubit revisited to enhance coherence and reproducibility, *Nature Communications* **7**, 10.1038/ncomms12964 (2016).
- [12] Y. Qiu, W. Xiong, X.-L. He, T.-F. Li, and J. Q. You, Four-junction superconducting circuit, *Scientific Reports* **6**, 10.1038/srep28622 (2016).
- [13] I. M. Pop, K. Geerlings, G. Catelani, R. J. Schoelkopf, L. I. Glazman, and M. H. Devoret, Coherent suppression of electromagnetic dissipation due to superconducting quasiparticles, *Nature* **508**, 369 (2014).
- [14] K. V. Shulga, E. Il'ichev, M. V. Fistul, I. S. Besedin, S. Butz, O. V. Astafiev, U. Hübler, and A. V. Ustinov, Magnetically induced transparency of a quantum metamaterial composed of twin flux qubits, *Nature Communications* **9**, 10.1038/s41467-017-02608-8 (2018).
- [15] M. Stern, G. Catelani, Y. Kubo, C. Grezes, A. Bienfait, D. Vion, D. Esteve, and P. Bertet, Flux qubits with long coherence times for hybrid quantum circuits, *Physical Review Letters* **113**, 10.1103/physrevlett.113.123601 (2014).
- [16] S. Gustavsson, F. Yan, J. Bylander, F. Yoshihara, Y. Nakamura, T. P. Orlando, and W. D. Oliver, Dynamical decoupling and dephasing in interacting two-level systems, *Physical Review Letters* **109**, 10.1103/physrevlett.109.010502 (2012).